Microstrip delay line phase shifter by actuating integrated ground plane membranes

C. Shafai, S.K. Sharma, J. Yip, L. Shafai and L. Shafai

Abstract: The design, simulation, fabrication, measurement and performance of a V-band microstrip delay line phase shifter using electrostatically actuated integrated micro-machined ground plane membranes are presented. The microstrip line is etched on an RFIC-friendly silicon substrate. The membrane is made of aluminium micro-ribbons and is fabricated on the ground plane side of the silicon substrate. The actuation of the ribbons away from the transmission line introduces an air gap between the radio-frequency (RF) substrate and the ground plane. By controlling the air gap thickness, a controllable phase shift in the transmission line is obtained. Each micro-ribbon measures 3.20 mm in length, 20 μm in width and 1 μm in thickness. A measured phase shift of 41° at 50 GHz was achieved with an actuation voltage of 120 V. The fabrication process added a 20 μm initial air gap between the micro-ribbons and RF substrate, increasing the required actuation voltage for a given phase shift. The simulated phase shift results agree well with the measurements.

1 Introduction

Phased array antennas are used for electronic beam steering and are implemented using radio-frequency (RF) phase shifters [1]. The RF phase shifters provide inter-element phase shifts, independent of the other system components, in the form of insertion phase delays. The most common type of phase shifters are based on ferrite materials, p–i–n diodes or field effect transistor switches. However, they introduce insertion loss that becomes significant at high gigahertz frequencies [2]. Recently, different micro-electro-mechanical (MEMS)-based phase shifters have also been demonstrated [3]. One type is the delay line phase shifter [4, 5], where the phase shift is achieved by routing the RF signal via switches to transmission lines (T-lines) of different lengths. The selection of different T-line segments allows for a change in the total length of the transmission line and thus results in a phase shift. This type of phase shifter allows for large, discrete phase shifts. Another type is the distributed micro-electro-mechanical transmission line (DMTL) MEMS phase shifter [6]. In this type, the transmission line is periodically loaded with MEMS bridges, acting as loading capacitors. By controlling the distributed capacitance on the line, the phase velocity and phase shift are controlled. The authors in [7] have shown a DMTL phase shifter for U-and W-band frequencies. The resulting phase shifter had a figure-of-merit (FOM) of 70°/dB at 40 GHz and 90°/dB at 60 GHz. These distributed line phase shifters perform well at very high frequencies (W-band and beyond). The authors in [8] demonstrated a MEMS phase shifter using copper corrugated membranes as the ground plane. A series of five 4.3 mm diameter membranes were used to achieve a 32.1° phase shift at 15.00 GHz along a 30 Ω line. A single 10.4 mm diameter membrane provided a phase shift of 55.5° at 14.25 GHz. The actuation voltage was 405 V, high for some applications. This actuation voltage can be reduced by reducing the required membrane deflection, or by improving the mechanical properties of the membrane itself. The latter was demonstrated in [9–10], where both simulated and measured results were presented.

This paper presents the design, simulation, fabrication, measurement and performance of a V-band microstrip delay line phase shifter using an integrated, voltage actuated, micro-machined ground plane membrane. The corrugated membranes used as ground plane in [8] are replaced by flexible micro-ribbons that require significantly lower actuation voltage. In Section 2, the theory of this type of phase shifters is described. Section 3 discusses the simulation results of the phase shifter against the membrane deflection. Section 4 contains the fabrication details of the membrane and the phase shifter device, as well as the simulated and measured results of the membrane deflection. In Section 5, the measurement results are verified for the fabricated delay line phase shifters at 50 GHz. This frequency was selected because it was the highest frequency we could accurately conduct the measurements. Simulations were carried out using Ansoft's high-frequency structure simulator (HFSS) [11] and COMSOL Multiphysics™ [12], both of which are finite-element method (FEM)-based full wave analysis programs.

2 Theory

Fig. 1 shows the geometry of the phase shifter, where micro-ribbons are fabricated below the microstrip line on a silicon

doi:10.1049/iet-map:20060197

Paper first received 14th August 2006 and in revised form 25th June 2007

C. Shafai, J. Yip and L. Shafai are with the Department of Electrical and Computer Engineering, The University of Manitoba, Winnipeg, Manitoba, Canada R3T 5V6

S.K. Sharma was InfoMagnetics Technologies Corporation, 900-330, St. Mary Avenue, Winnipeg, Manitoba, Canada R3C 3Z5 and the Department of Electrical and Computer Engineering, The University of Manitoba, Winnipeg, Manitoba, Canada R3T 5V6. He is currently with the Department of Electrical and Computer Engineering, San Diego State University, 5500 Campanile Drive, San Diego, California, CA 92182-1309, USA

L. Shafai was with the Carlton University, Ottawa, Ontario, Canada K1S 5B6. She is currently with the Electromagnetic Modelling Department of National Defence Quality Engineering Test Establishment (QETE 4-5-6) Ottawa, Ontario, Canada K1A 0K2

E-mail: shafai@ee.umanitoba.ca

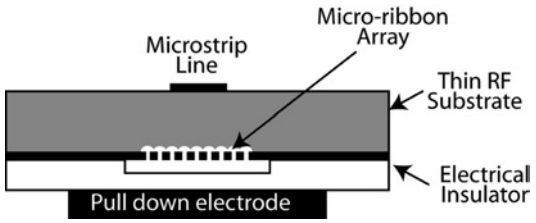

Fig. 1 *Schematic of the MEMS phase shifter utilising the aluminium micro-ribbon array*

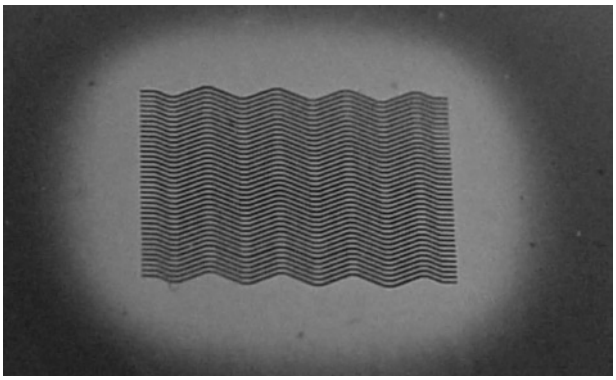

Fig. 2 *Array of fabricated micro-ribbons that span a 3.2 mm length*

substrate. A pull-down electrode placed below the ribbons is used to actuate the micro-ribbons away from the RF substrate, introducing a controllable air gap between the ribbons and the RF substrate. This allows controlling the effective permittivity of the substrate, and thus the phase shift. Fig. 2 shows an array of fabricated gold micro-ribbons. The ribbons are fabricated with undulation, to make them spring-like, and highly flexible. Each ribbon measures 3.2 mm long and 42 μm wide.

The phase velocity of the wave in a microstrip line is given by

$$\beta = \frac{c}{\sqrt{\varepsilon_{\text{eff}}}} \tag{1}$$

where β is the phase velocity, c the speed of light in vacuum and ε_{eff} the effective permittivity of the substrate. In this case, the effective permittivity is due to the stacked air (d_2) and silicon (d_1) as shown in Fig. 3.

The phase shift occurs because of the change in permittivity of the region between the transmission line and ground plane, due to the air gap. The effective permittivity ε_{eff} can be estimated from the addition of the dielectric capacitances in series as

$$\varepsilon_{\text{eff}} = \frac{\varepsilon_1 \varepsilon_2 (d_1 + d_2)}{\varepsilon_1 d_2 + \varepsilon_2 d_1} \tag{2}$$

where ε_1 and d_1 are the permittivity and thickness of the silicon wafer and ε_2 and d_2 are those of the air gap, respectively.

Figs. 4*a* and *b* show the differential phase shift and line impedance results obtained from an HFSS™ [11]

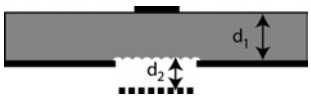

Fig. 3 *Schematic of the stacked dielectrics in the phase shifter setup*

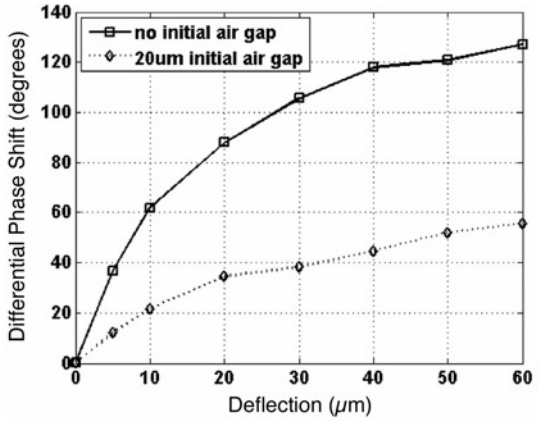

a

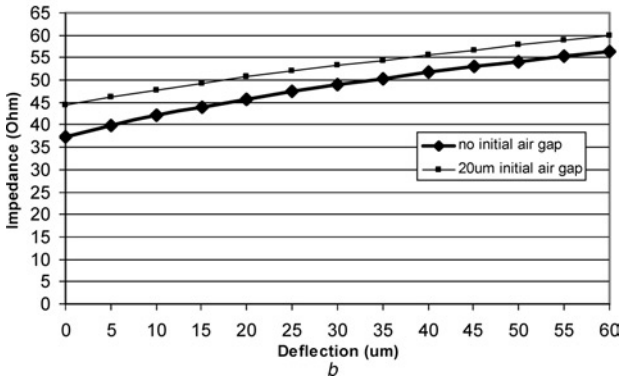

b

Fig. 4 *HFSS simulation results for a 3 mm transmission line at 50 GHz showing the*

a Magnitude of differential phase shift
b Line impedance performance with the variation of membrane deflection (t) for the two cases: case 1 with no initial air gap and case 2 with a 20 μm initial air gap

simulation of the structure. The differential phase shift is defined as the difference between the phase delays in the microstrip line without and with the air gap. A 3 mm long transmission line is modelled at 50 GHz. The substrate is silicon with $\varepsilon = 11.9$ and thickness of 250 μm. The transmission line impedance without the air gap was 37 Ω. Two cases are modelled: (1) with no initial air gap and (2) with 20 μm initial air gap and a silicon thickness of 230 μm. An evaluation of Fig. 4*a* shows that case 1 provides larger phase shifts, and about 125° with a uniform ribbon array deflection of 60 μm. A closer examination of (2) and Fig. 4*a* shows the importance of starting off with a minimal initial air gap. In case 1, the first 20 μm deflection causes ~90° phase shift, whereas in case 2 it causes only ~35° phase shift. Similarly, Fig. 4*b* shows the line impedance variation with the membrane deflection for the two cases, where it can be observed that case 2 impedance is higher than case 1 and is ~50 Ω. Further, the ribbon fabrication should avoid having large initial air gaps. In the fabrication process used for the device presented in this paper, the air gap was measured to be ~20 μm and was used in the simulations. Unfortunately, for a given phase shift, this air gap increases the required actuation voltage. Therefore an essential design criterion for this structure is to minimise the initial air gap, as this would reduce needed ribbon deflection for a given phase shift, and so require reduced actuation voltage.

3 Simulation results of delay line phase shifter

The simulation geometry of the phase shifter is shown in Fig. 5. A rectangular flat membrane is shown in Fig. 5*a*,

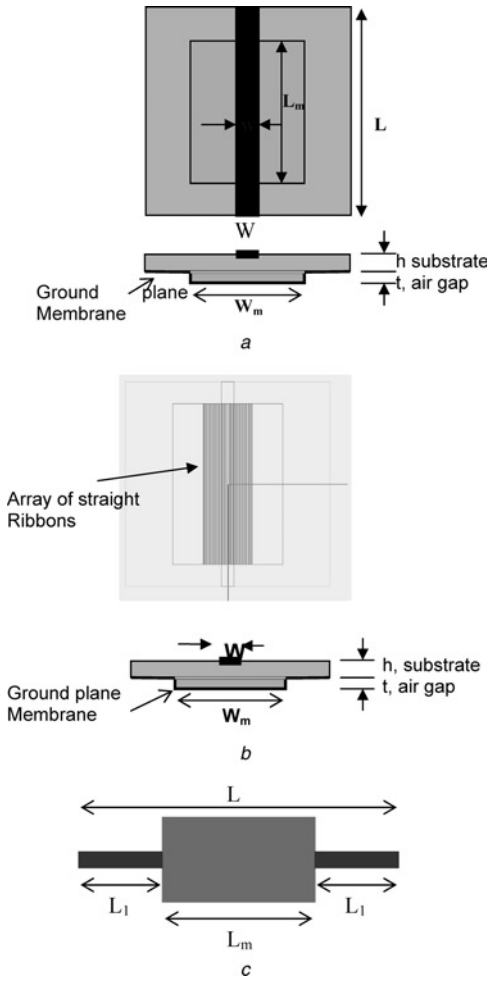

Fig. 5 *Geometry of the microstrip transmission delay line phase shifter with*

a Flat rectangular membrane
b Membrane made of straight ribbons
c Membrane (length L_m) below a transmission line (length L), leaving sections of length L_1 at each end

which is replaced by an array of ribbon structure in Fig. 5*b*. The selected substrate is silicon ($\varepsilon_r = 11.9$, $\rho = 0.001\ \Omega$ cm) of thickness, $h = 250\ \mu$m. The line length L is kept 6.50 mm for all simulations, so the membranes see the same line length as shown in Fig. 5*c*. Initially, a simpler configuration of flat membranes (Fig. 5*a*) of two different dimensions, $L_m \times W_m =$ 2.8 mm × 3.5 mm and 5.1 mm × 3.5 mm are selected. The microstrip line length and width are $L = 6.50$ mm and $W = 0.40$ mm, respectively. The line width corresponds to a 37 Ω line at zero membrane deflection ($t = 0\ \mu$m) and zero air gap. The computed return loss (S_{11}), insertion loss (S_{21}) and line loss, differential phase shift and FOM of the phase shifter are shown in Figs. 6*a*–*d*, respectively, at 50 GHz. The differential phase shift is defined as the difference between the initial phase shift and that after the deflection. The line loss is computed after subtracting the mismatch loss from the insertion loss. The FOM is defined as the absolute value of 'differential phase shift (°)/1 dB line loss'. The simulations were run considering an initial air gap of 20 μm as mentioned in the previous section and in Figs. 4*a* and *b*. This initial air gap is between the membrane and Si substrate and is limited only to the membrane area, beyond which the air gap is zero, where the line impedance is 37 Ω (Fig. 4*b*). This figure also shows that for the section of the line over the membrane, the air gap of 20 μm increases the line impedance to 45.8 Ω.

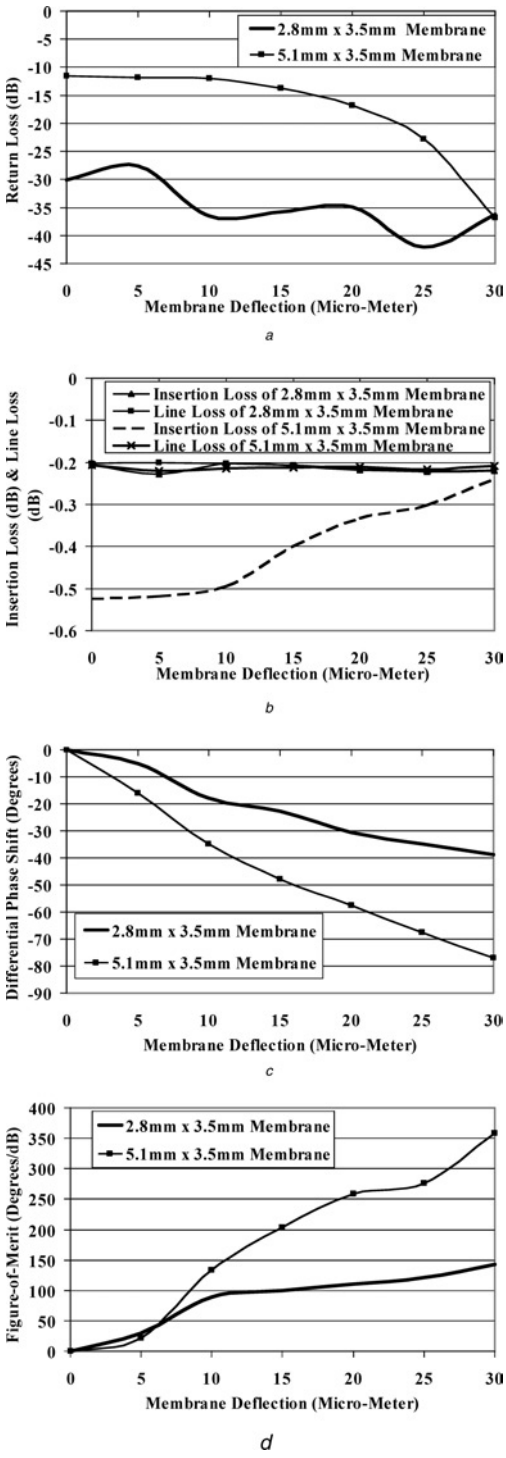

Fig. 6 *Simulated phase shifter performance*

a Return loss
b Insertion loss and line loss
c Differential phase shift
d FOM for the flat rectangular membrane at 50 GHz with the transmission line of length $L = 6.5$ mm, below which both 2.8 mm × 3.5 mm and 5.1 mm × 3.5 mm membranes are centrally placed

An observation of Fig. 6*a* reveals that the transmission line is impedance matched ($S_{11} = -10$ dB) for the membrane deflection from $t = 0$ to 30 μm, which is in addition to the initial air gap of 20 μm. The line length L is 6.5 mm and is larger than the membrane length L_m, as shown in Fig. 5*c*. Thus, there are two end sections of length L_1 on both sides of the membrane. The impedance of these end sections is 37 Ω but over the membrane it is variable and increases from 45.8 to 54.2 Ω (ε_{eff} changes from 5.819 to 4.607), as the

membrane deflection increases from 0 to 30 μm. In spite of these impedance variations, the line with small membrane remains well matched. For this membrane, the line segments are near multiples of half wavelengths and help in impedance matching. This is not the case for the larger membrane, but its impedance match is still satisfactory and improves with the membrane deflection. Since the total line length L is fixed at 6.5 mm, its resistive loss is almost invariant of the membrane deflection, as the variation of the line loss over the membrane is small compared with the overall line loss. However, the insertion loss varies as the impedance match (S_{11}) varies (Fig. 6*b*). It can be observed that the two membranes show similar line loss values, as the line length is the same for both membranes (Fig. 5*c*). The achieved differential phase shifts, for $t = 30$ μm deflection, are -39° and -77° for 2.8 mm × 3.5 mm and 5.1 mm × 3.5 mm membranes, respectively (Fig. 6*c*). The increase in phase shift is approximately proportional to the increase in membrane length L_m, from 2.8 to 5.1 mm for the same membrane deflection $t = 0$ to 30 μm. The computed FOM values are 143°/dB and 358°/dB at $t = 30$ μm, as shown in Fig. 6*d*. Note that, this is not the FOM of the membrane, as the line includes the extra sections L_1. For this reason, the larger membrane gives a higher FOM. In practice, if the two line sections L_1 could be eliminated, in phase shifter fabrication, the device FOM could increase even further to $\sim 450^\circ$/dB.

Fig. 7 shows the phase shifter performance with the variation in frequency for the impedance match (Fig. 7*a*) and differential phase shift (Fig. 7*b* for 30 μm deflection). The

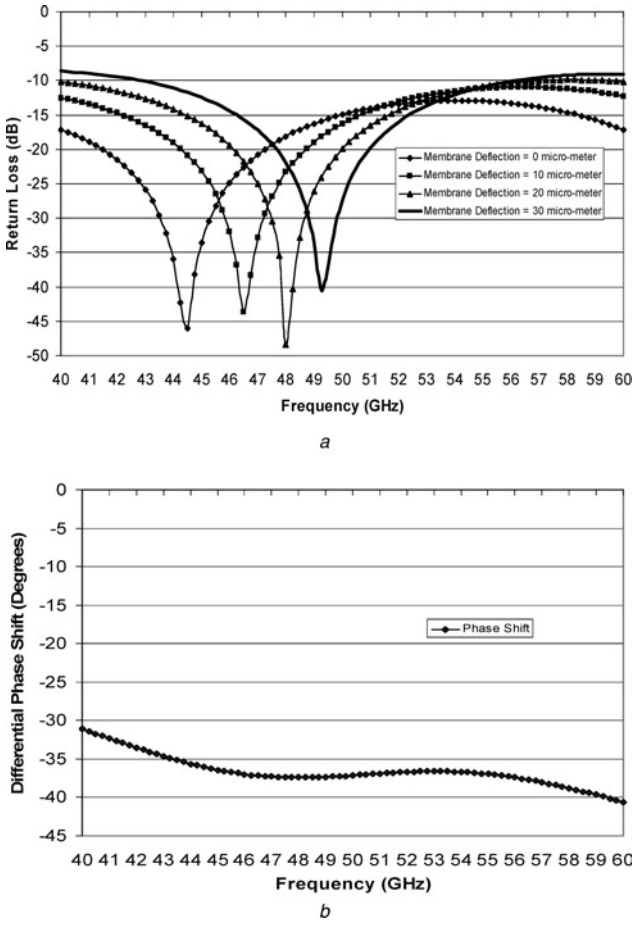

Fig. 7 *Simulated phase shifter performance against frequency for the flat rectangular membrane of Fig. 5, transmission line length L = 6.5 mm, 2.8 mm × 3.5 mm membrane centrally placed*

a Return loss
b Differential phase shift

return loss behaviour depends on the membrane deflection. For a given deflection, the insertion loss and variation of the differential phase depend on frequency. The latter changes rapidly at two ends, but is nearly constant at the centre. It should be noted, however, that this frequency response is for the three-section transmission line of Fig. 5, made of two line sections L_1 (37 Ω) and the membrane (varying impedance from 45.8 to 54.2 Ω). The membrane itself is a true delay line with a linear phase–frequency relationship. In practice, one can design the phase shifter section to provide a required, or intended, phase slope with frequency, which will depend on the overall line configuration including the port impedances.

The fabricated membranes used an array of meandering ribbons (as shown in Fig. 2), to facilitate mechanical deflection. However, for simplicity in the HFSS simulations, an array of straight ribbons was considered (width = 42 μm and inter-ribbon separation = 42 μm). Thus, the effects of meandering the ribbons on the line impedance characteristics were not studied in this paper. However, slight increase in the line loss is expected (about 8%), as path length is increased in the case of meandering ribbons. The number of ribbons was selected such that they extended beyond the fringing field. The simulation model is shown in Fig. 5*b*. The 2.8 mm × 3.5 mm membrane was selected for the investigation, as it showed better impedance match throughout the membrane deflection. Again, the simulations were run with an initial air gap of 20 μm, as discussed in Fig. 4. The return loss, the insertion and line loss, differential phase shift and FOM results are shown in Figs. 8*a*–*d*, respectively.

From Fig. 8*a*, it can be observed that the line is well matched initially, but S_{11} increases with deflection. Consequently, its insertion loss, starting around -0.25 dB, also increases (Fig. 8*b*). The line loss is shown in Fig. 8*b* and varies slightly around -0.25 dB, throughout the air gap variation. The maximum differential phase shift achieved is -39° (Fig. 8*c*), which is in agreement with the solid membrane result presented in Fig. 6*c*. The peak FOM value is 151°/dB line loss, as shown in Fig. 8*d*, near to that of the solid membrane. This study confirmed the electrical similarity of solid and ribbon membranes, and justifies their use for the phase shifter design. An increase in the differential phase shift can be obtained by making array of membranes as previously shown in [8]. To demonstrate it again, a two-element array was simulated with flat rectangular membrane case at 50 GHz. The achieved differential phase shift was twice that of the single membrane, presented in Figs. 6 and 8. However, these results are not included here for brevity.

4 Membrane fabrication and deflection results

4.1 Membrane simulation results

FEM simulations were done using the MEMS module in COMSOL Multiphysics™ [12]. The electrostatic force between the pull-down electrode and the micro-ribbons is a function of the capacitance between the two structures. The capacitance on each ribbon depends on the separation distance between the ribbon and the electrode, and also on its separation distance from the adjacent ribbons, the inter-ribbon separation, as this affects fringing. An investigation was first done to see the role of the inter-ribbon separation distance on the capacitance between the pull-down electrode and each micro-ribbon. A 2D simulation was performed along the central cross-section bisecting the length of the ribbon array for the case of 11 adjacent

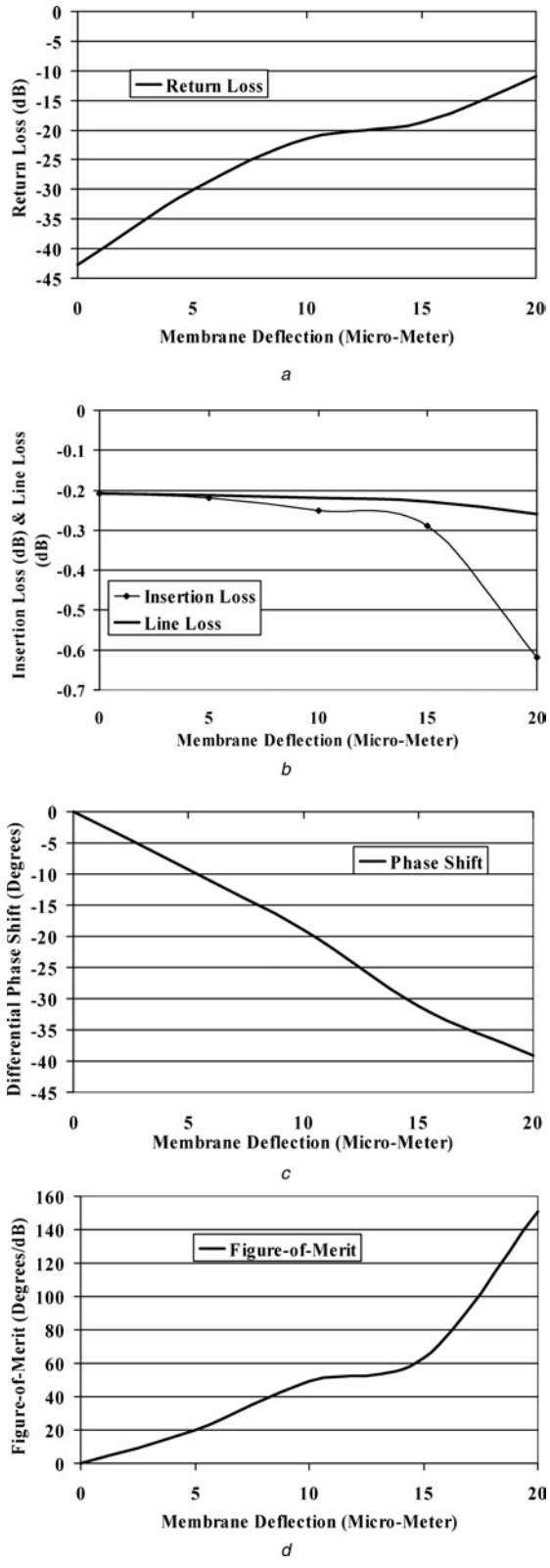

Fig. 8 *Phase shifter performance for the flat rectangular membrane of 2.8 mm × 3.5 mm size and employing the straight ribbons (as shown in Fig. 5b) at 50 GHz below a line length L = 6.50 mm*

a Return loss
b Insertion loss and line loss
c Differential phase shift
d FOM

micro-ribbons. The pull-down electrode was positioned 100 μm below the ribbon array and 50 V was applied to it. For simplicity, each micro-ribbon was assumed to be straight, rigid, 20 μm wide and 1 μm thick aluminium.

Table 1: Inter-ribbon separation in the array and the resulting electrostatic force

inter-ribbon separation, μm	electrostatic force, N/m
5	2.57×10^{-5}
10	3.00×10^{-5}
20	3.85×10^{-5}
40	5.37×10^{-5}
60	6.56×10^{-5}
80	8.23×10^{-5}
100	8.59×10^{-5}
200	12.4×10^{-5}

Table 1 shows the resulting electrostatic force. We can see the electrostatic force (and so capacitance) increases with the inter-ribbon separation distance, due to higher fringing. Thus, larger ribbon spacing will result in a lower actuation voltage being required to deflect the micro-ribbons. In practical implementation, larger inter-ribbon separation distance would also result in fewer ribbons and higher resistive losses, which could be an issue when passing RF signals. For the micro-ribbon array described later in this paper for experimental testing, an inter-ribbon spacing of 70 μm was fabricated, as this gave good balance with force increase, in relation to the number of ribbons in the array to ensure low RF losses.

Three-dimensional simulations were done in order to investigate how many segments in the micro-ribbon would give appropriate flexibility. The act of increasing the number of segments in the micro-ribbon can be viewed as increasing the number of segments in a spring; however, the length of each segment between jogs is shortened. In this set of simulations, all the ribbons spanned a distance of 3 mm, had a width of 20 μm and a thickness of 1 μm. The distance from the actuation electrode was 100 μm. A fixed electrostatic force of 1×10^{-7} N was applied in the simulation to each ribbon test case, and was distributed evenly along each ribbon. This level of force would result from approximately a 20 V applied to the pull-down electrode. The jog angle was 22.5°, where the jog angle, θ, is defined in Fig. 9. Table 2 shows the deflection of each micro-ribbon and its respective spring constant. As can be seen from Table 2, the straight beam is the stiffest, whereas the beam made up of two segments is the most flexible. However, a two-segmented ribbon was deemed inappropriate due to unsymmetrical twisting of the ribbon structure that would occur upon deflection. It can also be seen that there is not a very large difference in flexibility between the micro-ribbons that are made of 3–7 segments. However, as the number of segments increases, the micro-ribbon approaches the straight beam case. This means that a various numbers of segments can be chosen. For these cases, the surface area of the beam does not change significantly and thus the electrostatic force is the same as well.

4.2 Fabrication

A thin film of aluminium 1 μm in thickness is deposited onto a 250 μm thick silicon wafer via sputtering. The transmission line is then patterned (Fig. 10*a*). The transmission

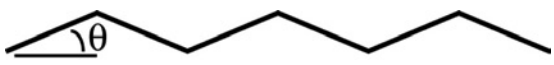

Fig. 9 *Illustration of the jog angle θ*

Table 2: Simulated spring constant of micro-ribbons of various numbers of segments with 0.1 μN applied force

no. of segments	spring constant, N/m
Straight	2.3×10^{-2}
2	0.20×10^{-2}
3	0.35×10^{-2}
4	0.44×10^{-2}
5	0.48×10^{-2}
6	0.52×10^{-2}
7	0.59×10^{-2}

line is 400 μm in width. The aluminium for the micro-ribbons is then deposited via a sputtering process on the other side of the wafer. The micro-ribbons are then patterned (Fig. 10*b*). The micro-ribbons are released from the underlying silicon wafer in gas etch. Different etch recipes, using XeF_2 gas and CF_4 plasma etch, were attempted in order to attain a nearly isotropic etch (Fig. 10*c*).

The geometry of the micro-ribbon can be seen in Fig. 11. The fabricated ribbons are 1 μm thick and 18 μm wide. The jog angle chosen was 22.5°. The ribbons span a length of 3.2 mm. The separation between the adjacent micro-ribbons in the array was 70 μm.

4.3 Deflection test results

The deflection of the fabricated micro-ribbons against pull-down electrode actuation voltage was investigated. Measurements were done with the micro-ribbons located 120 μm away from the electrode. The actuation voltage was increased by 10 V for each measurement. Micro-ribbon position was measured with a microscope, which was focused on the centre of a micro-ribbon. As deflection occurs, the microscope is refocused and the deflection measurement is read off the micrometer of the microscope. The position measurement accuracy of this technique is about ±3 μm. The deflection measurements are shown in Table 3. Comparison with simulation was not done. This is because the COMSOL simulation does not take into account the movement of the ribbon, as it

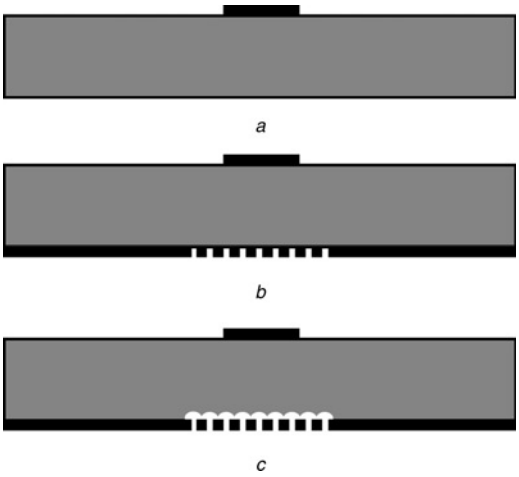

Fig. 10 *Fabrication process for the aluminium micro-ribbons*

a Deposit and pattern the transmission line
b Deposit and pattern the aluminium micro-ribbons
c Gas etch to release the micro-ribbons, which introduces an initial air gap into the system

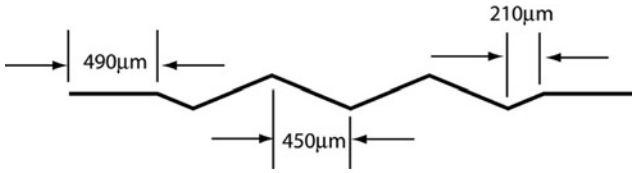

Fig. 11 *Dimensions of the fabricated ribbons*

The micro-ribbon was 20 μm in width and spanned a length of 3.2 mm

undergoes deflection when it calculates the electrostatic force on the ribbon. Thus, it under-predicts the ribbon motion when significant ribbon deflection occurs.

It should be noted that the spring constant and resonant frequency of the micro-ribbons vary significantly as a function of their deflection. This is due to the fact that the ribbons are fixed at both ends. For example, the structure of Fig. 11 when at rest (0 μm deflection) was simulated in COMSOL to possess a spring constant 1.2×10^{-3} N/m and a resonant frequency of 430 Hz. However, under application of 0.5 μN evenly distributed force, the micro-ribbon was simulated to deflect 34 μm at its centre. The resulting spring constant is 1.5×10^{-2} N/m and a resonant frequency increases to 1500 Hz.

5 Delay line phase shifter measurement results

The photograph of the fabricated phase shifter is shown in Fig. 12, as discussed in the previous section. The electrode for applying the actuation voltage is shown also, which is separated by a thin insulating material from the ground plane membrane. The measurements were carried out by placing the phase shifter in Anritsu's Test Fixture with V-connectors and ME7808A Network Analyzer in Antenna and Microwave Laboratory (AML) at the University of Manitoba.

The measured phase shift results by applying the actuation voltage from 0 to 120 V were obtained. The return loss and insertion (S_{21}) phase and differential phase shift results are shown in Figs. 13*a* and *b*, respectively, at 49.65 and 45 GHz. The return loss shows deterioration with the actuation voltage, but stays better than −8 dB throughout the actuation range in case of 49.65 GHz, whereas at 45 GHz it is always matched (Fig. 13*a*). It can also be seen that, with the actuation voltage up to 30 V, there is very little insertion phase and differential phase shift variations for both frequencies (Fig. 13*b*). The measured differential phase shifts for this actuation range variation are −41.14° and −41.63°, respectively, for 49.65 and 45 GHz. It can be seen that, in this frequency range, the phase shift varies very slowly with frequency as observed in Fig. 7*b*. The line loss and computed FOM values are −0.18 and −0.217 dB and 230.05°/dB and 191.84°/dB, respectively, at 49.65 and 45 GHz. The

Table 3: Deflection measurements for the fabricated ribbons

voltage, V	deflection, μm
60	26
70	33
80	42
90	48
100	58
110	69

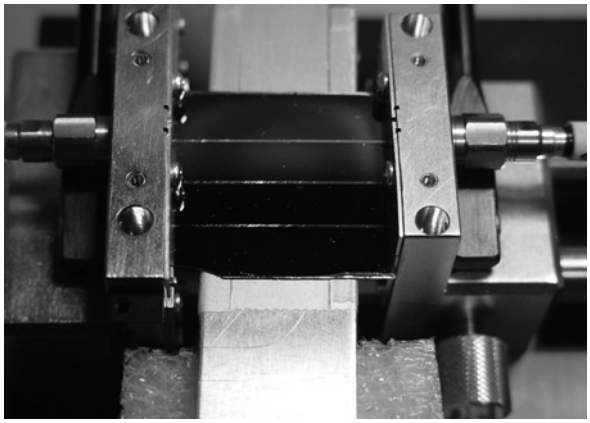

Fig. 12 *Membrane-actuated delay line phase shifter placed in test fixture with V-band connectors for feeding the line and an electrode below the ground plane for the electrostatic actuation of the membrane separated by a thin insulating material*

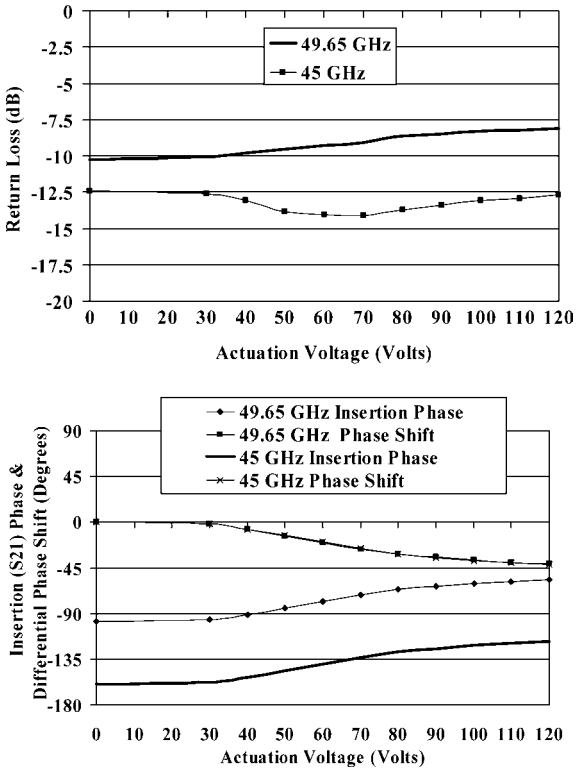

Fig. 13 *Measured delay line phase shifter results at 45 and 49.65 GHz showing*

a Return loss
b Insertion (S_{21}) phase and differential phase shift performances against the actuation voltage

comparison of the measured (49.65 GHz) results with the simulated (50 GHz) results employing the flat rectangular and straight ribbon membranes are shown in Table 4. It is evident that the simulation results agree well with the measured phase shifts, while the FOM value is slightly lower due to the increased line loss in the measurement, which is expected.

As mentioned earlier, a 20 μm initial air gap exists between the micro-ribbon membranes and the RF substrate as a result of the fabrication process used. This initial air gap reduces the phase shift performance as discussed earlier and in Fig. 4*a* by close to 90°. Future work will focus on reducing this initial air gap, as this would significantly increase the phase shifting performance of this device, as a function of ribbon actuation distance. Also, a reduced initial air gap would have the additional benefit of decreasing the needed membrane actuation voltage for a given desired phase shift value.

Table 4: Comparison of measured (49.65 GHz) differential phase shift and FOM performance with the simulated ones (straight ribbons and 50 GHz) for the flat rectangular membranes implemented microstrip delay lines

case	phase shift, °	FOM, °/dB	FOM, °/mm
measured with meander ribbon membrane	−41.14	230.05	−12.86
simulated with flat rectangular membrane	−38.81	331.27	−13.86
simulated with straight rectangular ribbon membrane	−39.13	350.72	−13.98

6 Conclusions

In this paper, the phase shift performance at V-band of a microstrip transmission line phase shifter is presented, which employs an integrated ground plane rectangular ribbon-type membrane on silicon substrate. Aluminium micro-ribbons were designed to lower the actuation voltage. The microstrip line and the micro-ribbons were fabricated onto the same silicon wafer. Aluminium micro-ribbons were fabricated on a 250 μm thick silicon wafer. The micro-ribbons were 3.2 mm in length, 20 μm in width and 1 μm thick. The separation distance between the individual micro-ribbons in the array was 70 μm and that lead to a force magnification. Phase shift measurements were done with the micro-ribbons spacing of 120 μm from the pull-down electrode. A 41° phase shift was achieved with an actuation voltage of 120 V at 50 GHz. Larger phase shifts can be achieved, with the same voltage, by decreasing the initial air gap or by using a sequence of multiple micro-ribbon arrays in the ground plane of the microstrip line. The use of micro-ribbons reduced the actuation voltage range to ∼100 V, lower than the 400 V of the previous work [8]. This will permit the use of membrane phase shifters in practical applications like in satellite and wireless communications. The measured phase shifts agreed well with the simulated results.

7 Acknowledgments

This work was supported by the Canadian Space Agency, InfoMagnetics Technologies Corporation and the Natural Sciences and Engineering Research Council (NSERC) of Canada.

8 References

1 Johnson, R.C., and Jasik, H.: 'Antenna engineering handbook' (McGraw-Hill, New York, 1984, 2nd edn.), Ch. 20
2 Koul, S.K., and Bhat, B.: 'Microwave and millimeter wave phase shifters' (Artech House, Norwood, MA, 1991), vol. I
3 Rebeiz, G.M.: 'RF MEMS: theory, design, and technology' (Wiley Inter-Science, NJ, USA, 2003)

4 Mihailovich, R.E., Kim, M., Hacker, J.B. *et al*.: 'MEM relay for reconfigurable RF circuits', *IEEE Microw. Wirel. Compon. Lett.*, 2001, **11**, pp. 53–55
5 Duffy, S., Bozler, C., Rabe, S. *et al*.: 'MEMS microswitches for reconfigurable microwave circuitry', *IEEE Microw. Wirel. Compon. Lett.*, 2001, **11**, pp. 106–108
6 Hung, J.-J., Dussopt, L., and Rebeiz, G.M.: 'Distributed 2- and 3-bit W-band MEMS phase shifters on glass substrates', *IEEE Trans. Microw. Theory Tech.*, 2004, **52**, (2), pp. 600–606
7 Barker, N.S., and Rebeiz, G.M.: 'Optimization of distributed MEMS transmission line phase shifters U-band and W-band designs', *IEEE Trans. Microw. Theory Tech.*, 2000, **48**, pp. 1957–1966
8 Shafai, C., Sharma, S.K., Shafai, L. *et al*.: 'Microstrip phase shifter using ground-plane reconfiguration', *IEEE Trans. Microw. Theory Tech.*, 2004, **52**, (1), pp. 144–153
9 Sharma, S.K., Shafai, C., and Shafai, L.: 'Performance of microstrip transmission line phase shifter with integrated ground plane membrane using low actuation voltage'. Proc. 12th Int. Symp. Antenna Technology and Applied Electromagnetics (ANTEM) and Canadian Radio Science (URSI/CNC), Montreal, QC, Canada, 16–19 July 2006, pp. 355–358
10 Yip, J., Shafai, C., Sharma, S.K. *et al*.: 'MEMS micro-ribbons in ground plane for microstrip phase shifter'. Proc. 12th Int. Symp. Antenna Technology and Applied Electromagnetics (ANTEM) and Canadian Radio Science (URSI/CNC), Montreal, QC, Canada, 16–19 July 2006, pp. 333–336
11 HFSS™ version 9.2.1, Ansoft Corporation, Pittsburgh, PA, USA, 2004
12 COMSOL Multiphysics™ version 3.2a, COMSOL AB, Stockholm, Sweden, 2005